Effect of Transition-Metal-Ion Dopants on the Oxygen Evolution Reaction on NiOOH(0001)

Journal:	*Physical Chemistry Chemical Physics*
Manuscript ID	CP-ART-05-2018-002849.R1
Article Type:	Paper
Date Submitted by the Author:	29-Jun-2018

Complete List of Authors:	Tkalych, Alexander; Princeton University, Dept. of Chemistry Martirez, John Mark; Princeton University, Mechanical and Aerospace Engineering Carter, Emily; Princeton University, Dept. of Mechanical and Aerospace Engineering

Effect of Transition-Metal-Ion Dopants on the Oxygen Evolution Reaction on NiOOH(0001)

Alexander J. Tkalych,[a] John Mark P. Martirez,[b] and Emily A. Carter[c,*]

[a] Department of Chemistry, Princeton University, Princeton, NJ 08544, USA

[b] Department of Mechanical and Aerospace Engineering, Princeton University, Princeton, NJ 08544, USA

[c] School of Engineering and Applied Science, Princeton University, Princeton, NJ 08544, USA

Abstract

Iron-doped nickel oxyhydroxide has been identified as one of the most active alkaline oxygen evolution reaction (OER) catalysts, exhibiting an overpotential lower than values observed for state-of-the-art precious metal catalysts. Several computational investigations have found widely varying effects of doping on the theoretical overpotential of the OER on NiO_x. Comparisons of these results is made difficult by the numerous differences in the structural and computational parameters used in these studies. In this work, within a consistent framework, we calculate the theoretical overpotentials for reactions occurring on the most stable, basal plane of undoped and doped β-NiOOH. We compare the activities of Fe(III), Co(III), and Mn(III) doping using density functional theory with Hubbard-like *U* corrections on the transition-metal *d* orbitals. We compare the effect of surface and subsurface doping in order to establish whether the dopants act as new active sites for the reaction or whether they induce more widespread changes in the material. The results of our study find only a small reduction in the overpotential (~0.1 and ≤ 0.05 V when doped in the surface and subsurface layers, respectively) for the three dopants, if doped in the dominant basal plane. This is much less than the reductions of 0.3 V experimentally observed for the most active Fe-doped systems. Furthermore, the magnitudes of reductions in overpotentials for the three dopants are similar. This work therefore disqualifies the possibility of enhancing the activity of the dominant exposed basal plane of β-NiOOH through substitutional doping.

Introduction

The need for alternative energy storage technologies has driven wide-ranging research in materials science. Of the numerous proposed technologies, the production of hydrogen *via* electrolytic water splitting offers the potential to store energy using a benign fuel cycle. In recent years, iron (Fe)-doped nickel oxyhydroxide (NiOOH) has emerged as one of the most promising materials to catalyze the most difficult part of the water splitting reaction: the oxygen evolution reaction (OER). Fe-doped NiOOH was first identified as a promising OER catalyst in 1987 by Corrigan.[1] This work demonstrated that inclusion of Fe in the NiOOH lattice adversely affects the charge storage reaction exploited in NiOOH-based batteries, in fact due to enhanced OER kinetics. Peak OER activities have been observed for a range of Fe-doping concentrations. The original study by Corrigan found that Fe-doping concentrations of about 10% led to the highest OER current densities.[1] Other studies achieved Fe-doping concentrations of up to 50% with little loss in OER performance. While Corrigan found the NiOOH lattice accommodates Fe concentrations of up to 75% without major structural modifications,[1] Louie and Bell concluded that the host structure was retained for doping concentrations of up to 90%.[2] Several other studies found that Fe dramatically improves the OER activity of NiOOH. Overpotentials at 10 mA cm^{-2} as low as 200-250 mV have been observed.[3–6] Furthermore, these systems are remarkably robust. Miller and Rocheleau found that the low overpotential characteristic of this system remained constant for over 7000 hours of operation.[7]

Like Fe, cobalt (Co) has been studied extensively as an additive to NiOOH. Co, unlike Fe, however, improves the performance of NiOOH battery cathodes. The addition of Co to the nickel hydroxide ($Ni(OH)_2$) crystals lowers the latter's oxidation potential.[8] Co also is thought to improve the performance of NiOOH cathodes by providing a conducting matrix of H_xCoO_2.

CoO(OH) is a d^6 system that is electrically insulating and exhibits no charge storage capacity. The formation of H_xCoO_2 ($x < 1$) produces of small amounts of Co^{4+}. If islands of H_xCoO_2 are connected, $Ni(OH)_2$ could be provided with conducting pathways that improve its overall conductivity. Co is introduced into the NiOOH lattice by cathodic co-deposition from a solution containing Co(II) and Ni(II).[9] Co then occupies the Ni lattice sites in $Ni(OH)_2$ and is quickly oxidized to Co(III).[10] Work done to study the effect of incorporation of Co into the NiOOH lattice has shown that Co doping leads to an OER overpotential as low as ~0.3 V.[11,12]

Mn has been studied only rarely as a dopant in NiOOH. Two investigations of Mn as a dopant to stabilize α-$Ni(OH)_2$ reached conflicting conclusions. Demourgues-Guerlou *et al*. observed that repeated cycling of Mn-doped α-$Ni(OH)_2$ led to dissolution of the material.[13,14] Their work also demonstrated that addition of Mn increases the oxidation potential of the cathode and decreases the OER overpotential relative to undoped NiOOH. Axmann and Glemser, unlike Demourgues-Guerlou *et al*., found excellent stability for 25% Mn-doped NiOOH.[15] This work also demonstrated that Mn substitutes directly for Ni in the NiOOH lattice.

Several groups have investigated the OER on both pure and doped NiOOH using density functional theory (DFT) with the Perdew-Burke-Ernzerhof (PBE)[16] generalized gradient approximation (GGA) functional with a Hubbard-like U correction for the transition-metal d-orbitals (DFT+U).[17] Li and Selloni calculated the OER overpotentials for pure and Fe-doped β-NiOOH$(01\bar{1}5)$, pure and Fe-doped γ-NiOOH(101), and $NiFe_2O_4$(001). Fe-doping of β-NiOOH was predicted to reduce the overpotential from 0.48 V to 0.26 V (using U_{Ni}= 5.5 eV, U_{Fe}= 3.3 eV).[18] They predicted that the OER on the pure and doped systems are potential-limited by formation of HO* and surface interstitial O_2*, respectively. Friebel *et al*. [19] calculated higher overpotentials for both pure and Fe-doped γ-NiOOH$(01\bar{1}2)$: 0.56 and 0.43 V, respectively

(using U_{Ni}= 6.6 eV, U_{Fe}= 3.5 eV), with a less impressive decrease upon introduction of Fe. In addition to examining a different surface, these overpotentials were calculated assuming a mechanism different from Li and Selloni, exhibiting OER potential-limiting steps of formation of O* and HOO* for the undoped and doped cases, respectively. Fidelsky and Toroker found that Fe-doping of β-NiOOH$(01\bar{1}5)$ reduced the overpotential from 0.61 V to 0.36 V (using U_{Ni}= 5.5 eV, U_{Fe}=3.3 eV) assuming the same mechanism as Li and Selloni.[20] Not surprisingly, this decrease is very similar to the prediction of Li and Selloni; the difference in calculated overpotentials is mostly due to Fidelsky and Toroker using a calculated thermodynamic potential for water oxidation (1.12 V) rather than the experimental value (1.23 V) used by Li and Selloni. By contrast, Doyle *et al*. found that Fe-doping of β-NiOOH(0001) only slightly reduced the overpotential from 0.43 V to 0.35 V (using U_{Ni}= 6.64 eV, U_{Fe}= 5.3 eV) *via* the HOO* associative pathway.[21] Finally, Costanzo predicted that Co-doping of β-NiOOH$(01\bar{1}5)$ reduces the OER overpotential even more than Fe, from 0.47 V to 0.18 V (U_{Ni}= 5.5 eV, U_{Co}= 3.0 eV), assuming the same mechanism proposed by Li and Selloni.[22] Fidelsky and Toroker also predicted that introducing OH vacancies at the β-NiOOH$(01\bar{1}5)$ surface would reduce the overpotential the most, from 0.61 V to 0.26 V (using U_{Ni}= 5.5 eV for Ni).[23]

Some DFT calculations that don't use a *U* correction for describing this process also have been reported. Goddard and co-workers used the hybrid functional B3PW91 together with microkinetic modeling to evaluate the effect of Fe-doping a γ-NiOOH(100) surface derived from a bulk structure proposed by Ceder and co-workers.[24] Goddard and coworkers predicted a 0.8 V reduction in the overpotential from 1.22 V to 0.42 V upon Fe-doping;[25] the overpotential here was defined as the applied potential that gives rise to a current density of 10 mA/cm^2 in their microkinetic model (using their calculated OER equilibrium potential of 1.06 V as a reference).

Recently, the same group used pure DFT-PBE to screen for dopants that might lower the overpotential further; they suggested that Co, Rh, and Ir would be even better than Fe for doping γ-NiOOH(100). Here the authors reverted to the conventional definition of theoretical overpotential (*vide infra*).[26] Given the significant inaccuracy of the PBE functional for treating these materials, these predictions clearly require follow-up with more reliable theory.

In most of these studies, $(01\bar{1}N)$-type surfaces were assumed, without evidence, to be the most active and therefore the most pertinent surface for OER. Taken all together, there are significant discrepancies in the predicted overpotentials for this material. These studies differ in structural models used, surfaces considered, and most notably OER mechanism(s) studied, in addition to differences in the *U* values used for the transition metals. These differences therefore motivate a comparative study in which the numerous variables (*e.g.*, calculation parameters, structural model) that can affect the overpotential are held constant.

To better understand the effect of dopants on the OER activity of NiOOH, this work seeks to compare the relative effects of Fe(III), Co(III), and Mn(III) as dopants when doped into the first or second layer (Figure 1). The work begins with the selection of an OER mechanism that is consistent with the experimentally determined overpotential for the undoped case. This model then is used to calculate the theoretical overpotential for each of the three dopants. This is done to establish whether the reduction in the overpotential observed for Fe is simply due to the availability of a new active site on the surface. This work also seeks to establish whether Co and Mn, transition-metal ions in close proximity to Fe in the periodic table, also manifest the experimentally observed enhancement effect.

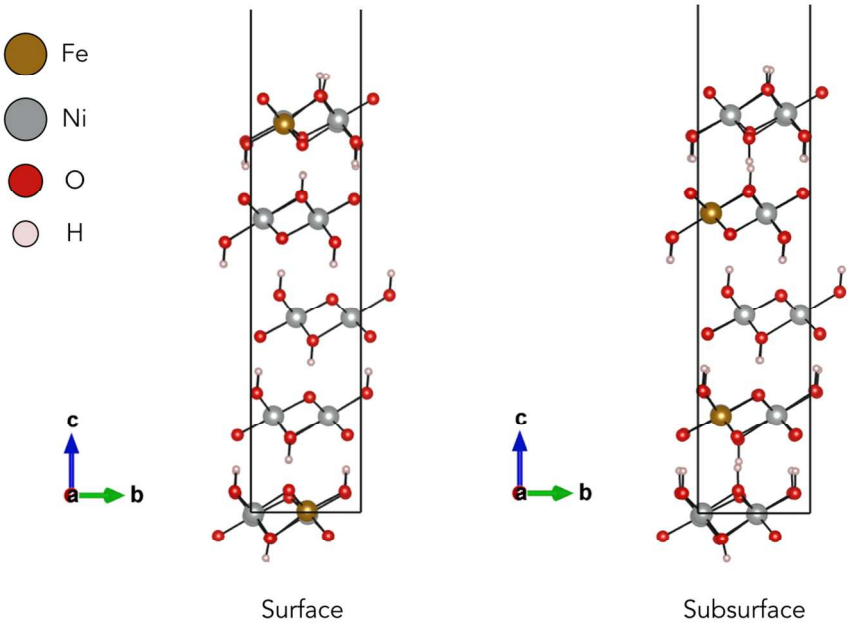

Figure 1: Side views of surface- and subsurface-doped β-NiOOH (0001) slabs (Fe-doped, in this case). Black boxes mark the supercell border. $\hat{a}$ and $\hat{b}$ are the in-plane bulk lattice vectors, and $\hat{c}$ is the vector normal to the surface ($\hat{a} \times \hat{b}$).

Computational details

We used the Vienna *Ab-initio* Simulation Package (VASP) version 5.3.3 to perform spin-polarized DFT+U calculations.[27–30] The DFT+U method[31,32] approximately addresses the spurious electron self-repulsion and missing derivative discontinuity in exchange-correlation (XC) that over-delocalizes electrons inherent to standard DFT. This allows for a more accurate treatment of first-row, transition-metal cations.[17,33] We used the PBE XC functional[16] in combination with the Dudarev *et al.* spherically invariant $U-J$ implementation.[17] We concluded earlier that a $U-J$ value of 5.5 eV for Ni(III), calculated using linear response theory by Li and Selloni,[18] leads to reasonably accurate replication of the structural and electronic properties of β-

NiOOH.[34] *U*–*J* values derived from electrostatically embedded Hartree-Fock theory of 4.3 eV,[35] 4.0 eV,[36] and 4.0 eV[37] were used for Fe(III), Co(III), and Mn(III), respectively. We employed Blöchl's all-electron, frozen-core, projector-augmented-wave (PAW) method.[38,39] Standard PAW potentials acted on the self-consistently optimized distributions of 3p/3d/4s electrons of Ni, Fe, Co, and Mn, 2s/2p electrons of O, and 1s electron of H. The total energy was converged to within 1 meV/atom using a plane-wave kinetic energy cutoff of 750 eV and Γ-point-centered Monkhorst-Pack *k*-point meshes[40] of 3 × 3 × 1 for a lateral 2 × 2 supercell containing five layers and 16 atoms/layer (*vide infra*).

Magnetic moments were determined from Löwdin atomic orbital projections. The magnetic moments were used subsequently to determine the oxidation state of the metals, based on the expected low- or high-spin configurations in an octahedral ligand field environment. Note that the atomic projection yields incomplete density projections, thus giving lower than expected, non-integer moments. However, the total spin density differences exhibit integer net spin moments that adhere to the expected summed-up spin moments of all the metals.

The ionic positions were allowed to relax to a force threshold of 0.01 eV $Å^{-1}$ during optimization, while the lattice parameters were fixed to their equilibrium bulk values using the equilibrium in-plane lattice vectors predicted recently for the lowest energy structure yet found for bulk β-NiOOH.[41] Gaussian smearing with a smearing width of 0.01 eV was used for integrating over the Brillouin zone for geometry optimizations. All final total energies were calculated using the tetrahedron method including Blöchl corrections to integrate the Brillouin zone.[42]

As the (0001) surface is the dominant facet exposed under electrochemical conditions,[43] we chose to study the OER on this surface. A vacuum layer of 15 Å introduced between the slabs

was found to be sufficient to minimize interactions between periodic images. To prevent dipole interactions within the slab, we used inversion symmetric surfaces. *A posteriori* dipole field and energy corrections in the direction perpendicular to the surface were applied to deal with residual dipole interactions between slabs; these energy corrections were negligible. We used slabs consisting of five NiOOH layers, containing 16 atoms/layer, for all calculations (with supercell dimensions of 5.894 Å × 5.984 Å × 36.000 Å). This thickness accurately replicates the bulk density in the middle (third) layer, suggesting that the surface layers experience a bulk-like electronic structure coming from the interior of the slab.[41]

Vibrational frequencies of each intermediate and of the surface-atom nearest-neighbors were calculated to determine whether the reaction intermediate structures were energy minima or saddle points. Numerical Hessian matrices were constructed from finite differences of displacements and force components on each atom. The Ni/O/H and dopant (except for subsurface substitutions) atoms in the first layer nearest to the reaction intermediate, and the atoms of the intermediate itself, were displaced by ±0.02 Å in all three directions from their equilibrium positions. The Hessian matrix resulting from these displacements then was diagonalized to yield vibrational frequencies corresponding to each normal mode. Only vibrational free energies for one side of the NiOOH slabs and adsorbates were included because the slabs have inversion symmetry and the Hessians are block diagonal with respect to each side of the slab (the displacement on one side does not affect the forces on the other side). All energies reported are for structures that have been confirmed to be true minima.

Enthalpic, $H(298\,K) - H(0\,K)$, and entropic, $S(298\,K)$, contributions for gas phase H_2O and H_2 (except for their DFT-calculated zero-point energies, $ZPEs$) and the condensation

free energy of H_2O, ΔG_{conds}^{exp}, were obtained from the NIST database[44] to determine the free energy of $H_2O(l)$ and $H_2(g)$:

$$G_{H_2O(l)} = E_{H_2O(g)}^{DFT} + ZPE_{H_2O(g)}^{DFT} + (H(298\,K) - H(0\,K) - TS(298\,K))_{H_2O(g)}^{exp} + \Delta G_{conds}^{exp}$$

$$G_{H_2(g)} = E_{H_2(g)}^{DFT} + ZPE_{H_2(g)}^{DFT} + (H(298\,K) - H(0\,K) - TS(298\,K))_{H_2(g)}^{exp}$$

The O_2(g) energy is known to be overbound by DFT-PBE by ~0.8 eV/O_2.[45] Therefore we define its energy as:

$$G_{O_2(g)} = 4.92\ \text{eV} + (2G_{H_2O(l)} - 2G_{H_2(g)})$$

where 4.92 eV is the negative of the experimental formation free energy of $H_2O(l)$ per O_2 at 298 K, also taken from the NIST database.[44]

Results and discussion

To examine the effect of dopants on the OER activity on β-NiOOH, we calculated the theoretical overpotential of a particular OER pathway on our slab models. The one-electron electrochemical elementary step with the largest free energy change determines the overall thermodynamics of the reaction. If the overall thermodynamic reaction potential (+1.23 V for the decomposition of water) is subtracted from the potential of the thermodynamically limiting step, the resulting quantity is the theoretical overpotential. This method of determining the OER activity was originally proposed in Ref. [46]. This value is a lower bound to the true overpotential for the reaction, as the experimental overpotential contains contributions from numerous departures from ideality, such as temperature effects, mass transfer limitations, and kinetic barriers.[47] Nevertheless, the theoretical overpotential is a useful metric for comparing activities of similar systems.

In previous work, we compared the theoretical overpotentials of four different proposed OER mechanisms on undoped β-NiOOH(0001).[48] This work accurately replicated the experimental overpotential (~0.5-0.6 V).[6,49] We also predicted that three of the four mechanisms had very similar overpotentials. Based on these results, we proposed that part of the difficulty faced by experimentalists in elucidating the OER mechanism on NiOOH is the possibility that numerous competing reactions may occur simultaneously on the same surface. In order to extend this work, we set out to examine the effect of various transition-metal dopants (Fe, Co, and Mn) to quantify their effect on the theoretical overpotential. Because of the similarity in overpotentials for three of the mechanisms we considered earlier (with the fourth mechanism much less thermodynamically favorable) and the large number of calculations required to compare different structural models, we focus here on the simplest of the three similar-overpotential mechanisms: the associative mechanism (*vide infra*). Although this mechanism did not exhibit the lowest of the theoretical overpotentials predicted earlier, the proximity of that overpotential to our lowest overpotential (less than 0.1 V difference) suggests that the model is well-suited for comparative studies.

The associative mechanism consists of six elementary steps (two chemical steps and four proton-electron transfer steps; see Table 1). The first step in the mechanism involves the formation of an O-O bond when a water molecule from solution adsorbs onto an oxygen atom in the NiOOH surface layer. This step assumes concomitant transfer of one of the water's protons to solution and transfer of one of the water's electrons to the NiOOH bulk, on the way to forming OOH* (**1**). Next, this OOH* loses its proton to solution and an electron to bulk NiOOH to form O_2* (**2**). The O_2* then desorbs (**3**), producing an oxygen vacancy in the surface layer. Another water molecule from solution then fills this vacancy (**4**); the adsorbed water then loses two

protons and two electrons over the course of the next two elementary steps (**5, 6**) to regenerate the resting state of the catalyst.

Table 1: Reaction free energies of each elementary step in the associative OER mechanism shown in Fig. 2 for different dopants. The reaction step index is listed in parentheses after the elementary step (first column). The three columns listed under "Surface" correspond to the reaction free energies for the elementary steps taking place on the surface-doped slabs. The three columns listed under "Subsurface" correspond to the reaction free energies for the elementary steps taking place on the subsurface-doped slabs. The final column lists the reaction free energies for the elementary steps taking place on the undoped slab. The theoretical overpotential is in parentheses next to the largest free energy change, which is for step (**1**) in all cases.

Reaction step	Reaction free energies (eV)						
	Surface			Subsurface			Undoped
	Fe	Co	Mn	Fe	Co	Mn	
$O^* + H_2O \rightarrow OOH^* + (H^+ + e^-)$ (**1**)	1.73 (0.50)	1.74 (0.51)	1.70 (0.47)	1.79 (0.56)	1.81 (0.58)	1.75 (0.52)	1.80 (0.57)
$OOH^* \rightarrow O_2^* + (H^+ + e^-)$ (**2**)	0.99	1.11	1.26	1.04	1.06	1.09	1.22
$O_2^* \rightarrow O_2$ (**3**)	0.49	0.52	0.64	0.35	0.59	0.43	0.34
$H_2O \rightarrow H_2O^*$ (**4**)	-0.33	-0.30	-0.31	-0.22	-0.45	-0.31	-0.25
$H_2O^* \rightarrow OH^* + (H^+ + e^-)$ (**5**)	0.56	0.54	0.21	0.60	0.51	0.54	0.49
$OH^* \rightarrow O^* + (H^+ + e^-)$ (**6**)	1.48	1.32	1.43	1.37	1.39	1.44	1.32

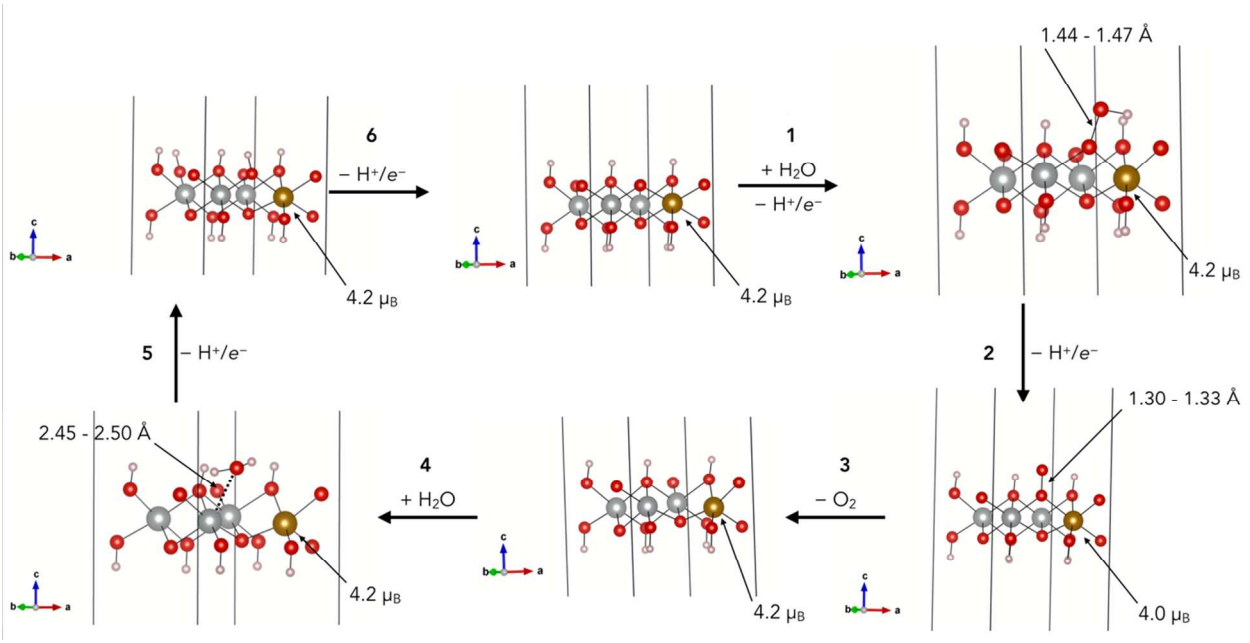

Figure 2: Side views of the reaction intermediates and one of the outermost slab layers considered in this particular OER pathway on β-NiOOH (0001) showing octahedrally coordinated transition-metal cation sites. This example corresponds to the surface-Fe(III)-doped NiOOH slabs. The atom-projected magnetization of the Fe at each elementary step and ranges in pertinent bond lengths due to different substituents at several steps are displayed. Black boxes mark the supercell border. Note that the surface oxygen vacancy after the third step is in between the Fe and Ni atoms.

Numerous studies have examined dopant concentration effects on the OER activity of NiOOH. For Fe dopants in particular, these reports claim optimal performance at Fe-doping concentrations ranging from 10 – 50%, with several concluding that concentrations of ~25% produce peak performance.[1,2,49–51] We therefore considered a surface doping concentration of 25% for all of our doped systems. Considerable debate exists in the literature as to whether the

dopant improves the performance of the host structure by serving as the new active site or because of rearrangements in the structural and electronic properties of the surrounding Ni ions. To examine this phenomenon, we employed two different structural models (see Figure 1 for side views of each). In the first model, we doped the outermost surface layer on each side of the slab with 25% Fe, Co, or Mn. In the second, we left the outermost surface layers undoped and instead doped the layers – one on each side of the slab – immediately below each surface layer with 25% Fe, Co, or Mn. We doped only a single layer on each side of the slab at a time to isolate the effects of surface and subsurface doping.

Despite a slight reduction (~0.1 V, Table 1) in the theoretical overpotential for the mechanism and basal plane surfaces considered here, we do not observe the dramatic reduction (~0.3 V) measured in numerous experiments on Fe-doped NiOOH.[3] The theoretical overpotential determined on undoped β-NiOOH, 0.57 V, is consistent with experiments performed on pristine β-NiOOH (*i.e.*, when special precautions are undertaken to avoid Fe-contamination).[6] Subsurface doping has little effect on the theoretical overpotential of this system; all theoretical overpotentials were within 0.05 V of the undoped value. We note here that these results are qualitatively consistent with recent work by Doyle *et al*. who found that surface Fe-doping of β-NiOOH(0001) reduced the overpotential by ~0.1 V (from 0.43 V to 0.35 V), looking at the same mechanism presented herein. The discrepancy in the absolute overpotentials results from a variety of factors, including the use of different structural models and calculation parameters. Specifically, their slab model was thinner (three layers), they used a lower kinetic energy cutoff (400 eV), their force convergence threshold was less stringent (0.05 eV $Å^{-1}$), and they employed different U values for Ni and Fe than in the present work: U_{Ni} = 6.64 eV and U_{Fe} = 5.3 eV. The

lowest theoretical overpotential predicted here, for surface-Mn(III)-doped β-NiOOH, is only 0.1 V less than that of undoped β-NiOOH.

This result is in contrast to Li and Selloni's finding of a reduction in the theoretical overpotential of 0.22 V when comparing Fe-doped β-NiOOH($01\bar{1}5$) to undoped β-NiOOH($01\bar{1}5$).[18] This latter result was substantiated by Fidelsky and Toroker who found a reduction of 0.25 V in the OER overpotential also on the Fe-doped β-NiOOH($01\bar{1}5$).[20] A reduction in the theoretical overpotential of 0.29 V was replicated by Costanzo on Co-doped β-NiOOH($01\bar{1}5$) when considering the same pathway.[22] We note that all three of these studies considered a pathway involving a sterically-inaccessible near-surface O_2* interstitial. Friebel *et al*., looking at a closely-related facet, however, found a reduction in the overpotential of only 0.09 V due to Fe doping when considering the well-studied associative OOH* pathway.[19] Taken altogether, the studies reporting overpotentials close to those measured rely on the O_2* interstitial as the key intermediate species, although its existence has yet to be proven experimentally. The O_2* interstitial, however, is demonstrably more sterically hindered to form on six-fold metal sites of (0001). The theoretical overpotential for Fe-doped β-NiOOH (0001), routinely found to be one of the most effective OER catalysts discovered so far, is only slightly (0.07 V) less than the undoped value. The findings of our study demonstrate that, when holding all variables other than the dopant identity constant, the overpotentials for both the doped and undoped systems are nearly the same for OER on the basal plane of β-NiOOH. This work therefore disqualifies the possibility of enhancing the activity of the dominant exposed basal plane of β-NiOOH through substitutional doping.

The predicted dopant oxidation states (based on the atom-projected magnetic moments, or from total moments; see Figure 2, for example) remain largely unchanged throughout the

steps of the mechanism (from atom-projected moments we have 4.2 μ_B for Fe(III); 3.0 μ_B for Co(III); 3.2 μ_B for Mn(III)). Instead, changes occur in the oxidation states of the oxygenated intermediates (also assessed from their atom-projected magnetic moments). The magnetic moment on the adsorbed hydroperoxyl (OOH*) in step **1** is 0.0 μ_B, decreasing to −1.0 μ_B for adsorbed superoxo (O_2*) in step **2**. The dioxygen desorption step **3** yields an oxygen vacancy and concomitant partial reduction of two Ni ions from +3 to +2 adjacent to the vacancy (atom-projected S_z = 1.7 μ_B from 1.2 μ_B prior to reduction). Steps **5** and **6** involve two one-electron oxidation steps that recover the resting state of the catalyst. The small difference in overpotentials predicted for the doped versus undoped materials is consistent with the negligible change in dopant oxidation states during the reaction. These dopants do not affect the mechanism electronically by acting as redox-active species for the oxygen-derived intermediates, a phenomenon that is normally expected for an OER catalyst.[52]

These results strongly suggest that the substantial reduction in overpotential measured for Fe-doped NiOOH is more involved than simply the availability of a new active site or a rearrangement of the structural and electronic properties of the Ni ions surrounding the dopant. The appearance of a particularly active surface facet or a bias towards a substantially more active pathway could be responsible for the actual OER process. Edge sites on MoS_2, for example, are considerably more active for hydrogen evolution than sites on the basal plane.[53] Research to identify new, more active surface facets, however, must contend with results found by several groups that NiOOH film preparation conditions do not play an outsized role in the ultimate activity of the system. As an example, research by Landon *et al*. demonstrated that, despite synthesis conditions producing effective surface areas differing by a factor of three, the activities of the films produced were essentially the same.[51] One promising explanation is that synthetic

conditions leading both to the uptake of certain dopants (*e.g.*, Fe) and the formation of the hydrated, amorphous γ-NiOOH phase result in the highly active systems observed in experiment.[49,54]

Summary and Conclusions

In this work, we compared the theoretical overpotentials for the OER occurring on undoped and doped NiOOH basal planes. We first described and justified our choice of structural model considered and particular OER mechanism selected. We examined the effect of both surface and subsurface doping of Fe(III), Co(III), and Mn(III), comparing the theoretical overpotentials calculated for each of these systems with the value calculated for undoped NiOOH. Neither surface nor subsurface doping of any of the dopants produced the dramatic reduction in overpotential found experimentally for Fe-doped NiOOH. Surface doping produced a maximum reduction in the theoretical overpotential of 0.1 V for Mn-doped NiOOH, while subsurface doping yielded a maximum reduction of 0.05 V, again for Mn-doped NiOOH. The reduction in measured overpotential thus depends on more than simply the appearance of a new active site on this surface. This study therefore demonstrates that doping of Fe, Co, and Mn in the dominant basal plane of β-NiOOH does not lead to the large reductions in the overpotential found experimentally. Furthermore, no significant difference in theoretical overpotentials between the three dopants is found. The insubstantial reduction predicted here for the basal plane strongly suggests that the enhancement in OER activity, in particular the enhancement brought about by Fe, is largely occurring on minority facets, which is the subject of ongoing work in our group.

Associated Content

Electronic Supporting Information

Optimized geometries are provided.

Author information

Corresponding Author

* E-mail: eac@princeton.edu

Conflicts of interest

There are no conflicts to declare.

Acknowledgements

This article is based upon work supported by the Air Force Office of Scientific Research under AFOSR Award No. FA9550-14-1-0254. We acknowledge use of the TIGRESS high performance computer center at Princeton University. We also acknowledge the High Performance Computing Modernization Program of the US Department of Defense for providing additional computational resources. We also thank Ms. Nari Baughman and Dr. Johannes M. Dieterich for critical reading of this manuscript.

References

(1) Corrigan, D. A. *J. Electrochem. Soc.* **1987**, *134* (2), 377.

(2) Louie, M. W.; Bell, A. T. *J. Am. Chem. Soc.* **2013**, *135* (33), 12329.

(3) Gong, M.; Dai, H. *Nano Res.* **2015**, *8* (1), 23–39.

(4) Song, F.; Hu, X. *Nat. Commun.* **2014**, *5*, 1–9.

(5) Gong, M.; Li, Y.; Wang, H.; Liang, Y.; Wu, J. Z.; Zhou, J.; Wang, J.; Regier, T.; Wei, F.; Dai, H. *J. Am. Chem. Soc.* **2013**, *135* (23), 8452–8455.

(6) Klaus, S.; Cai, Y.; Louie, M. W.; Trotochaud, L.; Bell, A. T. *J. Phys. Chem. C* **2015**, *119* (13), 7243–7254.

(7) Miller, E. L.; Rocheleau, R. E. *J. Electrochem. Soc.* **1997**, *144* (9), 3072.

(8) Ohitani, M.; Takayama, T.; Takashima, K.; Tsuji, S. *J. Appl. Electrochem.* **1986**, *16*, 403.

(9) Balasubramanian, M.; Melendres, C. A.; Mini, S. *J. Phys. Chem. B* **2000**, *104*, 4300.

(10) Kim, M.; Kwang-Bum, K. *J. Electrochem. Soc.* **1998**, *145* (2), 507.

(11) Wang, H. Y.; Hsu, Y. Y.; Chen, R.; Chan, T. S.; Chen, H. M.; Liu, B. *Adv. Energy Mater.* **2015**, *5* (10), 1–8.

(12) Jiang, J.; Zhang, A.; Li, L.; Ai, L. *J. Power Sources* **2015**, *278*, 445.

(13) Guerlou-Demourgues, L.; Denage, C.; Delmas, C. *J. Power Sources* **1994**, *52* (2), 269–274.

(14) Guerlou-Demourgues, L.; Delmas, C. *J. Electrochem. Soc.* **1996**, *143* (2), 561–566.

(15) Axmann, P.; Glemser, O. *J. Alloys Compd.* **1997**, *246* (1–2), 232–241.

(16) Perdew, J. P.; Burke, K.; Ernzerhof, M. *Phys. Rev. Lett.* **1996**, *77* (18), 3865–3868.

(17) Dudarev, S. L.; Botton, G. A.; Savrasov, S. Y.; Humphreys, C. J.; Sutton, A. P. *Phys. Rev. B* **1998**, *57* (3), 1505–1509.

(18) Li, Y.; Selloni, A. *ACS Catal.* **2014**, *4*, 1148.

(19) Friebel, D.; Louie, M. W.; Bajdich, M.; Sanwald, K. E.; Cai, Y.; Wise, A. M.; Cheng, M.-J.; Sokaras, D.; Weng, T.-C.; Alonso-Mori, R.; Davis, R. C.; Bargar, J. R.; Norskov, J. K.; Nilsson, A.; Bell, A. T. *J. Am. Chem. Soc.* **2015**, *137*, 1305.

(20) Fidelsky, V.; Toroker, M. C. *Phys. Chem. Chem. Phys.* **2017**, *19* (11), 7491–7497.

(21) Doyle, A. D.; Bajdich, M.; Vojvodic, A. *Catal. Letters* **2017**, *147* (6), 1533–1539.

(22) Costanzo, F. *Phys. Chem. Chem. Phys.* **2016**, *18* (10), 7490–7501.

(23) Fidelsky, V.; Toroker, M. C. *J. Phys. Chem. C* **2016**, *120*, 25405.

(24) Van der Ven, a.; Morgan, D.; Meng, Y. S.; Ceder, G. *J. Electrochem. Soc.* **2006**, *153* (2), A210.

(25) Xiao, H.; Shin, H.; Goddard III, W. A. *Proc. Natl. Acad. Sci.* **2018**, *115* (23), 5872 LP-5877.

(26) Shin, H.; Xiao, H.; Goddard III, W. A. *J. Am. Chem. Soc.* **2018**, *140* (22), 6745–6748.

(27) Kresse, G.; Hafner, J. *Phys. Rev. B* **1993**, *47* (1), 558.

(28) Kresse, G.; Hafner, J. *Phys. Rev. B* **1994**, *49* (20), 14251.

(29) Kresse, G.; Furthmüller, J. *Phys. Rev. B* **1996**, *54* (16), 11169.

(30) Kresse, G.; Furthmüller, J. *Comput. Mater. Sci.* **1996**, *6* (1), 15–50.

(31) Anisimov, V. I.; Zaanen, J.; Andersen, O. K. *Phys. Rev. B* **1991**, *44* (3), 943–954.

(32) Liechtenstein, A. I.; Anisimov, V. I.; Zaanen, J. *Phys. Rev. B* **1995**, *52* (8), R5467.

(33) Cohen, A. J.; Mori-Sánchez, P.; Yang, W. *Science* **2008**, *321* (5890), 792 LP-794.

(34) Tkalych, A. J.; Yu, K.; Carter, E. A. *J. Phys. Chem. C* **2015**, *119* (43), 24315–24322.

(35) Mosey, N. J.; Liao, P.; Carter, E. A. *J. Chem. Phys.* **2008**, *129* (1), 14103.

(36) Ritzmann, A. M.; Pavone, M.; Muñoz-García, A. B.; Keith, J. A.; Carter, E. A. *J. Mater.*

Chem. A **2014**, *2* (21), 8060–8074.

(37) Pavone, M.; Ritzmann, A. M.; Carter, E. A. *Energy Environ. Sci.* **2011**, *4* (12), 4933.

(38) Blöchl, P. E. *Phys. Rev. B* **1994**, *50* (24), 17953.

(39) Kresse, G.; Joubert, D. *Phys. Rev. B* **1999**, *59* (3), 1758.

(40) Monkhorst, H. J.; Pack, J. D. *Phys. Rev. B* **1976**, *13* (12), 5188.

(41) Martirez, J. M. P.; Carter, E. A. *submitted,* **2018**.

(42) Blöchl, P. E.; Jepsen, O.; Andersen, O. K. *Phys. Rev. B* **1994**, *49* (23), 16223.

(43) Sac-Epee, N.; Palacin, M.; Delahaye-Vidal, A.; Chabre, Y.; Tarascon, J. *J. Electrochem. Soc.* **1998**, *145* (5), 1434.

(44) Chase, M. W.; Davies, C. A.; Downey, J. R.; Frurip, D. J.; McDonald, R. A.; Syverud, A. N. *NIST JANAF Thermochemical Tables 1985*; National Institute of Standards and Technology: Gaithersburg, MD, 1986.

(45) Ritzmann, A.; Muñoz-Garcia, A.; Pavone, M.; Keith, J.; Carter, E. *MRS Commun.* **2013**, *3*, 161–166.

(46) Nørskov, J. K.; Rossmeisl, J.; Logadottir, A.; Lindqvist, L.; Lyngby, D.-; Jo, H. *J. Phys. Chem. B* **2004**, *108*, 17886.

(47) Doyle, R. L.; Godwin, I. J.; Brandon, M. P.; Lyons, M. E. G. *Phys. Chem. Chem. Phys.* **2013**, *15* (33), 13737–13783.

(48) Tkalych, A. J.; Zhuang, H. L.; Carter, E. A. *ACS Catal.* **2017**, *7* (8), 5329–5339.

(49) Trotochaud, L.; Young, S. L.; Ranney, J. K.; Boettcher, S. W. *J. Am. Chem. Soc.* **2014**, *136* (18), 6744.

(50) Trotochaud, L.; Ranney, J. K.; Williams, K. N.; Boettcher, S. W. *J. Am. Chem. Soc.* **2012**, *134* (41), 17253.

(51) Landon, J.; Demeter, E.; Nilay, I.; Keturakis, C.; Wachs, I. E.; Vasic, R.; Frenkel, A. I.; Kitchin, J. R. *ACS Catal.* **2012**, *2*, 1793.

(52) Artero, V.; Fontecave, M. *Chem. Soc. Rev.* **2013**, *42* (6), 2338–2356.

(53) Jaramillo, T. F.; Jørgensen, K. P.; Bonde, J.; Nielsen, J. H.; Horch, S.; Chorkendorff, I. *Science* **2007**, *317* (5834), 100 LP-102.

(54) Bediako, D. K.; Lassalle-Kaiser, B.; Surendranath, Y.; Yano, J.; Yachandra, V. K.; Nocera, D. G. *J. Am. Chem. Soc.* **2012**, *134* (15), 6801.

TOC and summary

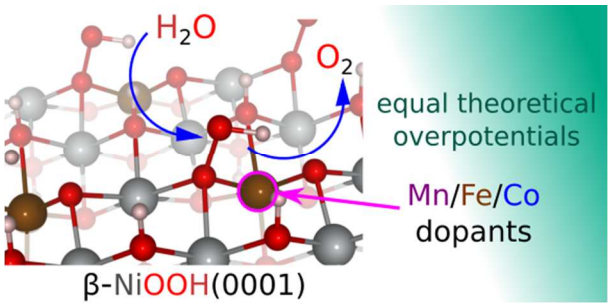

Contrary to experiments, transition-metal doping of the β-NiOOH(0001) surface does not accelerate oxygen evolution, suggesting other surfaces dominate the catalysis.